

Approximative two-flavor framework for neutrino oscillations with nonstandard interactions

Mattias Blennow*

Max-Planck-Institut für Physik, Föhringer Ring 6, 80805 München, Germany

Tommy Ohlsson†

*Department of Theoretical Physics, School of Engineering Sciences,
Royal Institute of Technology (KTH) – AlbaNova University Center,
Roslagstullsbacken 21, 106 91 Stockholm, Sweden*

Abstract

In this paper, we develop approximative two-flavor neutrino oscillation formulas including sub-leading nonstandard interaction effects. Especially, the limit when the small mass-squared difference approaches zero is investigated. The approximate formulas are also tested against numerical simulations in order to determine their accuracy and they will probably be most useful in the GeV energy region, which is the energy region where most upcoming neutrino oscillation experiments will be operating. Naturally, it is important to have analytical formulas in order to interpret the physics behind the degeneracies between standard and nonstandard parameters.

*blennow@mppmu.mpg.de

†tommy@theophys.kth.se

I. INTRODUCTION

Neutrino oscillation physics has had a remarkable progress as the leading description for neutrino flavor transitions during the last decade. Even though it serves as the leading description, other mechanisms could be responsible for transitions on a subleading level. In this paper, we will develop an approximative framework for neutrino oscillations with so-called nonstandard interactions (NSIs) as such subleading effects. This framework is derived in the limit when the small mass-squared difference is negligible, *i.e.*, $\Delta m_{21}^2 \rightarrow 0$, as well as when the effective matter interaction part of the Hamiltonian has only one eigenvalue significantly different from zero. The main effects of NSIs will be parametrized by v and β , which will be defined in Sec. III.

Recently, NSIs with matter have attracted a lot of attention in the literature. In some sense, the potential for these interactions can be viewed as a generalization of the coherent forward-scattering potential, which describes the effects of ordinary (or standard) interactions with matter [1], and indeed, gives rise to the famous Mikheyev–Smirnov–Wolfenstein (MSW) effect [1, 2, 3]. Especially interesting are approximative frameworks that consider neutrino oscillations with NSIs which could be used for atmospheric neutrino data in the ν_μ - ν_τ sector, since these data are sensitive to interactions of tau neutrinos [4, 5]. However, there are also other experimental situations, where one could investigate tau neutrino interactions such as with the MINOS experiment [6, 7, 8]. In addition, in Ref. [9], the authors have studied an approximative two-flavor neutrino scenario that is similar to our framework, but instead used for the OPERA experiment. Nevertheless, one should be aware of the fact that NSI effects are subleading effects and have been experimentally constrained [10, 11].

The paper is organized as follows. In Sec. II, we present the general scheme for three-flavor neutrino oscillations including NSIs. Next, in Sec. III, we develop an approximative two-flavor neutrino oscillation framework including subleading NSI effects as well as we compare our framework with earlier results. Then, in Sec. IV, we analyze our framework numerically. In Sec. V, we study applications to experiments. Finally, in Sec. VI, we summarize our results and present our conclusions.

II. NONSTANDARD INTERACTIONS IN NEUTRINO OSCILLATIONS

Standard three-flavor neutrino oscillations in vacuum can be described by the following Hamiltonian in flavor basis:

$$H_0 = \frac{1}{2E} U \text{diag}(0, \Delta m_{21}^2, \Delta m_{31}^2) U^\dagger, \quad (1)$$

where E is the neutrino energy, $\Delta m_{ij}^2 \equiv m_i^2 - m_j^2$ is the mass-squared difference between the i th and j th mass eigenstate, and U is the leptonic mixing matrix. By adding the effective matter Hamiltonian

$$H_{\text{matter}} \simeq \text{diag}(\sqrt{2}G_F N_e, 0, 0) = V \text{diag}(1, 0, 0) \quad (2)$$

to the vacuum Hamiltonian H_0 , standard matter effects on neutrino oscillations can be studied. In order to investigate the effects of NSIs between neutrinos and other fermions, another more general effective interaction Hamiltonian can be added. This effective Hamiltonian will be of the form

$$H_{\text{NSI}} = V \begin{pmatrix} \varepsilon_{ee} & \varepsilon_{e\mu} & \varepsilon_{e\tau} \\ \varepsilon_{e\mu}^* & \varepsilon_{\mu\mu} & \varepsilon_{\mu\tau} \\ \varepsilon_{e\tau}^* & \varepsilon_{\mu\tau}^* & \varepsilon_{\tau\tau} \end{pmatrix}, \quad (3)$$

where

$$\varepsilon_{\alpha\beta} = \sum_{f,a} \varepsilon_{\alpha\beta}^{fa} \frac{N_f}{N_e},$$

N_f is the number of fermions of type f , and we have assumed an unpolarized medium. Thus, the full Hamiltonian is given by

$$H = H_0 + H_{\text{matter}} + H_{\text{NSI}}, \quad (4)$$

which describes three-flavor neutrino oscillations in matter including NSIs.

III. REDUCTION TO TWO-FLAVOR EVOLUTION

Since the experimental bounds on $\varepsilon_{\mu\alpha}$ and $\varepsilon_{\alpha\mu}$ are relatively stringent [10], we focus on the case where the interaction part of the Hamiltonian takes the form

$$H_{\text{int}} = H_{\text{matter}} + H_{\text{NSI}} = V \begin{pmatrix} 1 + \varepsilon_{ee} & 0 & \varepsilon_{e\tau} \\ 0 & 0 & 0 \\ \varepsilon_{e\tau}^* & 0 & \varepsilon_{\tau\tau} \end{pmatrix} = V U_{\text{NSI}} \text{diag}(v, 0, \xi) U_{\text{NSI}}^\dagger, \quad (5)$$

where the unitary matrix

$$U_{\text{NSI}} = \begin{pmatrix} c_\beta & 0 & s_\beta e^{i\phi} \\ 0 & 1 & 0 \\ -s_\beta e^{-i\phi} & 0 & c_\beta \end{pmatrix}$$

defines the matter interaction eigenstates, $c_\beta = \cos(\beta)$, $s_\beta = \sin(\beta)$, and V is the standard MSW potential. In this framework, the NSIs are parametrized by the two matter interaction eigenvalues v and ξ as well as the matter interaction basis parameters β and ϕ and we have

$$\varepsilon_{ee} = v c_\beta^2 + \xi s_\beta^2 - 1, \quad \varepsilon_{e\tau} = s_\beta c_\beta e^{i\phi} (\xi - v), \quad \varepsilon_{\tau\tau} = v s_\beta^2 + \xi c_\beta^2. \quad (6)$$

Thus, the standard neutrino oscillation framework is recovered with $\beta = \xi = 0$ and $v = 1$.

From the results of atmospheric neutrino experiments, we know that even high-energy ν_μ oscillate, leading to $\xi \ll 1$ [4, 5] for the matter composition of the Earth. We will here consider the limit $Vv \sim \Delta m_{31}^2/(2E) \gg V\xi$, which is the applicable limit for standard neutrino oscillations with energies of a few GeV to tens of GeV inside the Earth, while earlier papers [4, 5] have studied the limit $Vv \gg \Delta m_{31}^2/(2E) \sim V\xi$. In the limit of $\xi \rightarrow 0$ and $\Delta m_{21}^2/(2E) \rightarrow 0$, the full three-flavor Hamiltonian takes the form (up to an irrelevant addition proportional to unity)

$$H = \Delta a_\Delta a_\Delta^\dagger + V v a_\nu a_\nu^\dagger, \quad (7)$$

where

$$a_\Delta = \begin{pmatrix} s_{13} e^{-i\delta} \\ s_{23} c_{13} \\ c_{23} c_{13} \end{pmatrix} \quad \text{and} \quad a_\nu = \begin{pmatrix} c_\beta \\ 0 \\ -s_\beta e^{-i\phi} \end{pmatrix}$$

are the third column of the leptonic mixing matrix U and first column of the matter interaction mixing matrix U_{NSI} , respectively. Since this Hamiltonian is defined using only two linearly independent vectors, a_Δ and a_ν , there must be a third linearly independent vector a_0 for which $H a_0 = 0$ and which is orthogonal to a_Δ and a_ν . The components of this vector are given by

$$a_0 = \frac{1}{c'} a_\Delta \times a_\nu, \quad (8)$$

where $c' = \cos(\theta')$ is a normalization factor with $\sin(\theta') = |a_\Delta^\dagger a_\nu|$ and we have introduced the product

$$(A \times B)_i = \varepsilon_{ijk} A_j^* B_k^*, \quad (9)$$

which is orthogonal to both A and B as well as antilinear in both arguments. With our parametrization, we have

$$s'^2 = (s_{13}c_\beta - c_{13}s_\beta c_{23})^2 + c_{23} \sin(2\beta) \sin(2\theta_{13}) \sin^2\left(\frac{\phi + \delta}{2}\right). \quad (10)$$

Since a_0 is an eigenvector of the full Hamiltonian regardless of the matter density, its evolution decouples from that of the other two states and it will only receive a phase factor. Thus, it will be possible to describe the evolution of the two remaining states in an effective two-flavor framework. Indeed, if we choose the basis

$$a_x = e^{i\alpha_x} a_v, \quad a_y = e^{i\alpha_y} a_v \times a_0 \quad (11)$$

(note that a_y is already normalized as a_v and a_0 are orthonormal), with α_x and α_y chosen such that $a_\Delta^\dagger a_x$ and $a_\Delta^\dagger a_y$ are real, then the two-flavor Hamiltonian in this basis takes the form

$$H_2 = Vv \begin{pmatrix} 1 & 0 \\ 0 & 0 \end{pmatrix} + \Delta \begin{pmatrix} s'^2 & s'c' \\ s'c' & c'^2 \end{pmatrix}, \quad (12)$$

which is an ordinary two-flavor Hamiltonian in matter with the vacuum mixing angle θ' , the mass-squared difference Δm_{31}^2 , and the MSW potential Vv . In order to compute the neutrino flavor evolution in this basis, any method applicable to two-flavor neutrino oscillations can be used.

While the above framework makes it easy to reduce the three-flavor evolution to a two-flavor evolution in the given basis, the final results have to be projected onto the flavor basis, where

$$\nu_e = \begin{pmatrix} 1 \\ 0 \\ 0 \end{pmatrix}, \quad \nu_\mu = \begin{pmatrix} 0 \\ 1 \\ 0 \end{pmatrix}, \quad \nu_\tau = \begin{pmatrix} 0 \\ 0 \\ 1 \end{pmatrix}. \quad (13)$$

The two bases are related by a unitary matrix V , which is given by

$$V_{\alpha i} = \nu_\alpha^\dagger a_i. \quad (14)$$

With this notation and the full evolution matrix given by

$$S = e^{i\Phi} \begin{pmatrix} e^{-i\Phi} & 0 & 0 \\ 0 & S_{xx} & S_{xy} \\ 0 & -S_{xy}^* & S_{xx}^* \end{pmatrix} \quad (15)$$

in the a_i basis, the general neutrino oscillation probability becomes

$$\begin{aligned}
P_{\alpha\beta} = & |V_{\beta 0}V_{\alpha 0}^*|^2 + (|V_{\beta x}V_{\alpha x}^*|^2 + |V_{\beta y}V_{\alpha y}^*|^2)P_{xx} \\
& + (|V_{\beta x}V_{\alpha y}^*|^2 + |V_{\beta y}V_{\alpha x}^*|^2)P_{xy} \\
& + 2 \operatorname{Re} \left[V_{\beta 0}V_{\alpha 0}^* e^{-i\Phi} \sqrt{P_{xx}} (V_{\beta x}^*V_{\alpha x} e^{i\Lambda_x} + V_{\beta y}^*V_{\alpha y} e^{-i\Lambda_x}) \right] \\
& + 2 \operatorname{Re} \left[V_{\beta 0}V_{\alpha 0}^* e^{-i\Phi} \sqrt{P_{xy}} (V_{\beta x}^*V_{\alpha y} e^{i\Lambda_y} - V_{\beta y}^*V_{\alpha x} e^{-i\Lambda_y}) \right] \\
& + 2 \operatorname{Re} \left[P_{xx}V_{\beta x}V_{\alpha x}^*V_{\beta y}^*V_{\alpha y} e^{-2i\Lambda_x} - P_{xy}V_{\beta x}V_{\alpha y}^*V_{\beta y}^*V_{\alpha x} e^{-2i\Lambda_y} \right] \\
& + 2\sqrt{P_{xx}P_{xy}} \operatorname{Re} \left[V_{\beta x}V_{\beta y}^* (|V_{\alpha y}|^2 - |V_{\alpha x}|^2) e^{-i(\Lambda_x + \Lambda_y)} \right] \\
& + 2\sqrt{P_{xx}P_{xy}} \operatorname{Re} \left[V_{\alpha x}^*V_{\alpha y} (|V_{\beta x}|^2 - |V_{\beta y}|^2) e^{-i(\Lambda_x - \Lambda_y)} \right], \tag{16}
\end{aligned}$$

where $S_{xx} = \sqrt{P_{xx}}e^{-i\Lambda_x}$ and $S_{xy} = \sqrt{P_{xy}}e^{-i\Lambda_y}$ (with this notation P_{xx} is the two-flavor survival probability and P_{xy} is the two-flavor transition probability).

From the above, it becomes apparent that the final neutrino oscillation probabilities are quite complicated unless further assumptions are made. This is mainly due to the fact that it is necessary to project the evolution matrix onto the flavor basis. In the case of $\beta = 0$, we regain the result from ordinary neutrino oscillations where $a_\nu = \nu_e$ and the ν_e survival probability takes a very simple form, *i.e.*, $P_{ee} = P_{xx}$. For simplicity, we present the analytic results only for the case $\delta = \phi = 0$, where the matrix elements $V_{\alpha i}$ are taken to zeroth order in s_{13} . This simplification will not lead to any large errors, since V is fixed and s_{13} is small. However, we keep $s_{13} \neq 0$ in the definition of θ' , since there can be resonance effects in the two-flavor evolution. The resulting neutrino oscillation probabilities are then given by

$$\begin{aligned}
c_0'^4 P_{ee} = & s_{23}^4 s_\beta^4 + c_\beta^4 \left\{ P_{xx} + 4c_0'^2 s_\beta^2 c_{23}^2 [P_{xy} \sin^2(\Lambda_y) - P_{xx} \sin^2(\Lambda_x)] \right. \\
& \left. + 4\sqrt{P_{xx}P_{xy}} c_0' s_\beta c_{23} (2c_0'^2 - 1) \sin(\Lambda_x) \sin(\Lambda_y) \right\} \\
& + 2s_{23}^2 s_\beta^2 c_\beta^2 \left\{ \sqrt{P_{xx}} [\cos(\Lambda_x - \Phi) - 2s_\beta^2 c_{23}^2 \sin(\Phi) \sin(\Lambda_x)] \right. \\
& \left. + 2\sqrt{P_{xy}} c_0' s_\beta c_{23} \sin(\Lambda_y) \sin(\Phi) \right\}, \tag{17}
\end{aligned}$$

$$c_0'^4 P_{\mu\mu} = c_\beta^4 c_{23}^4 + P_{xx} s_{23}^4 + 2\sqrt{P_{xx}} c_\beta^2 c_{23}^2 s_{23}^2 \cos(\Lambda_x + \Phi), \tag{18}$$

$$\begin{aligned}
c_0'^4 P_{e\mu} = & c_\beta^2 s_{23}^2 \left\{ P_{xy} + 2s_\beta^2 c_{23}^2 [P_{xx} - \sqrt{P_{xx}} \cos(\Lambda_x + \Phi)] \right. \\
& \left. + 2c_0' s_\beta c_{23} \sqrt{P_{xy}} [\cos(\Lambda_y + \Phi) - \sqrt{P_{xx}} \cos(\Lambda_x - \Lambda_y)] \right\}, \tag{19}
\end{aligned}$$

$$\begin{aligned}
c_0'^4 P_{\mu\tau} = & s_{23}^2 \left\{ c_\beta^4 c_{23}^2 \left[\left(1 - \sqrt{P_{xx}}\right)^2 + 4\sqrt{P_{xx}} \sin^2\left(\frac{\Lambda_x + \Phi}{2}\right) \right] + s_\beta^2 c_0'^2 P_{xy} \right. \\
& \left. + 2\sqrt{P_{xy}} c_\beta^2 s_\beta c_{23} c_0' [\cos(\Lambda_y - \Phi) - \sqrt{P_{xx}} \cos(\Lambda_x + \Lambda_y)] \right\}, \tag{20}
\end{aligned}$$

where $c_0'^2 = 1 - s_\beta^2 c_{23}^2$. The five remaining probabilities can be trivially deduced from the above results using unitarity conditions. Note that Eqs. (17)–(20) will be illustrated below in Figs. 1–5.

A. Comparison and consistency with earlier results

As mentioned above, in Refs. [4, 5], the limit of $v \rightarrow \infty$ and $\xi V \sim \Delta m_{31}^2/(2E)$ is studied. They also study the limit of $\xi \rightarrow 0$, which becomes similar to the approach taken in Ref. [12], where the limit of large matter effects was studied (the difference being that the former includes NSIs and the latter includes the effects of nonzero θ_{13} and Δm_{21}^2). In this limit, the eigenstate a_ν decouples, and since $V_{\mu x} = 0$, the ν_μ oscillates in a pure vacuum two-flavor system. It is found that the effective neutrino oscillation parameters in this system are given by

$$\Delta m_m^2 = \Delta m_{31}^2 \sqrt{[c_{2\theta}(1 + c_\beta^2) - s_\beta^2]^2/4 + s_{2\theta}^2 c_\beta^2}, \quad (21)$$

$$\tan(2\theta_m) = \frac{2s_{2\theta}c_\beta}{c_{2\theta}(1 + c_\beta^2) - s_\beta^2}, \quad (22)$$

where $c_{2\theta} = \cos(2\theta_{23})$ and $s_{2\theta} = \sin(2\theta_{23})$.

In our framework, it is easy to obtain the corresponding quantities as

$$\begin{aligned} \Delta m_m^2 &= 2E(a_y^\dagger H a_y - a_0^\dagger H a_0) \\ &= \Delta m_{31}^2 c'^2, \end{aligned} \quad (23)$$

$$\begin{aligned} \tan(\theta_m) &= |V_{\mu y}|/|V_{\mu 0}| \\ &= \frac{c_{13}s_{23}}{c_{13}c_\beta c_{23} + s_\beta s_{13}}, \end{aligned} \quad (24)$$

where the last equality holds only when $\phi = \delta = 0$ and becomes more complicated when this is not the case. It is easy to show that these results are the same as those of Refs. [4, 5] in the limit of $\theta_{13} \rightarrow 0$, where we obtain

$$\Delta m_m^2 = \Delta m_{31}^2 (1 - s_\beta^2 c_{23}^2), \quad (25)$$

$$\tan(\theta_m) = \frac{\tan(\theta_{23})}{c_\beta}, \quad (26)$$

which are slightly simpler forms of Eqs. (21) and (22). Note that Eqs. (23) and (24) are valid for any value of θ_{13} , whereas Eqs. (21) and (22) are only valid in the limit $\theta_{13} \rightarrow 0$. Our results also agree with those of Ref. [12] in the limit of no NSIs and $\Delta m_{21}^2 \ll \Delta m_{31}^2$.

Parameter	Value
Δm_{31}^2	$2.7 \cdot 10^{-3} \text{ eV}^2$
Δm_{21}^2	$8 \cdot 10^{-5} \text{ eV}^2$
θ_{12}	33.2°
θ_{23}	45°
θ_{13}	0 or 8°

TABLE I: The neutrino oscillation parameters used in our numerical examples. The value of θ_{13} is specified in each figure. In addition, for all examples, we have used $\delta = 0$.

IV. NUMERIC ANALYSIS OF OSCILLATION PROBABILITIES

In this section, we present numerical results to show the accuracy of the two-flavor approximation presented in the previous section. In order to perform this, we will present the neutrino oscillation probabilities in terms of neutrino oscillograms of the Earth, *i.e.*, probability iso-contours in the zenith-angle–neutrino-energy plane. Since we are mainly interested in the accuracy of the approximation (rather than making quantitative predictions), we use a simplified Earth model, where the mantle and core are approximated as having constant matter densities (4.65 g/cm^3 and 10.2 g/cm^3 , respectively). For the standard neutrino oscillation parameters, we have used the values given in Table I.

As will be observed in Figs. 1–5, the approximations of Eqs. (17)–(20) are surprisingly accurate in describing the shapes of the oscillograms, the main source of error coming from the negligence of the small mass-squared difference Δm_{21}^2 (putting $\Delta m_{21}^2 = 0$ in the numerical simulations would lead to differences between the approximations and the numerical results which would be hardly noticeable).

We will also observe that, in all cases, the NSI terms dominate the high-energy behavior of the neutrino oscillation probabilities, as expected. However, in addition, it will be apparent that the effective two-flavor mixing angle θ' plays a large role in determining the qualitative behavior at energies around the resonance energy. This includes discussions on where the resonance appears (both in energy and baseline), as well as on other resonant effects such as parametric resonance [13, 14, 15, 16, 17, 18]. For energies lower than the ones displayed in Figs. 1–5, our approximation will become worse due to the fact that the effects of Δm_{21}^2 will no longer be negligible.

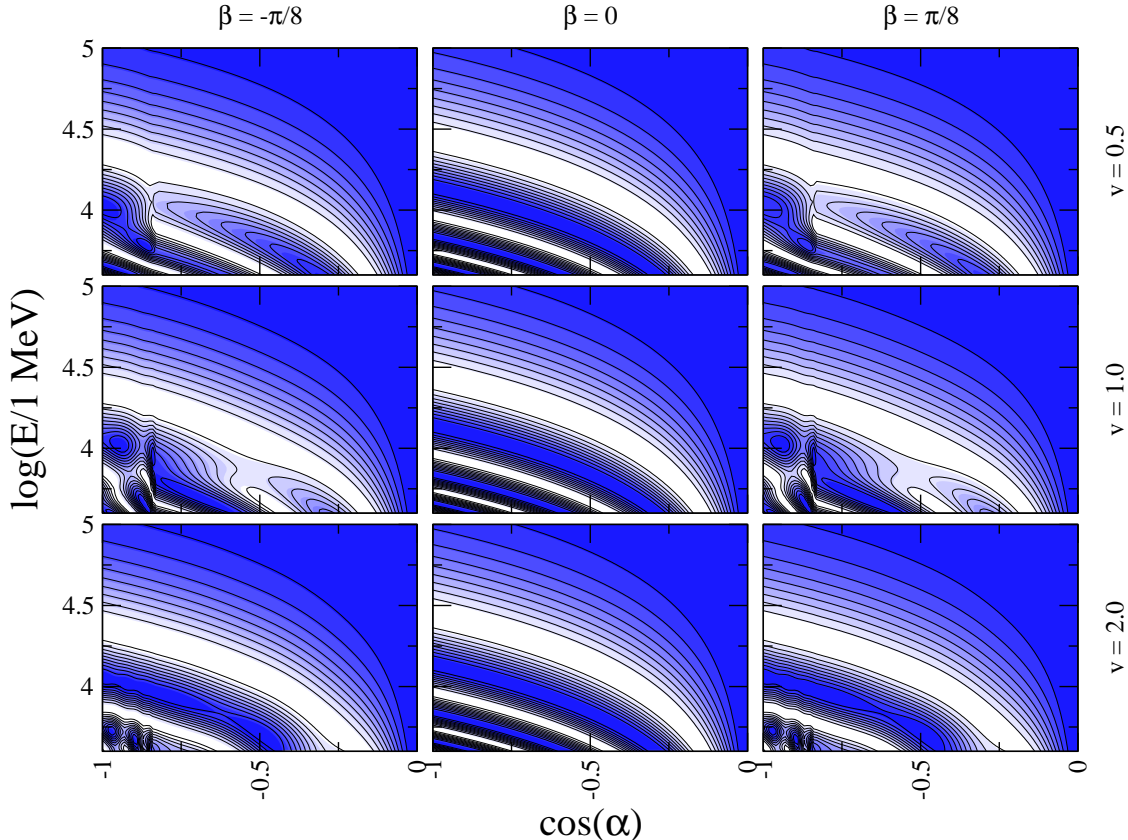


FIG. 1: The muon neutrino survival probability $P_{\mu\mu}$ as a function of zenith angle and energy for different values of ν and β . The colored regions correspond to the numerical results (darker regions for higher probability), while the solid black curves correspond to the two-flavor approximation introduced in Sec. III. In this figure, the leptonic mixing angle θ_{13} is set to zero.

A. The muon neutrino survival probability $P_{\mu\mu}$

In the next section, we will study the muon neutrino disappearance channel at a neutrino factory using the General Long Baseline Experiment Simulator (GLOBES). Thus, our first numerical example, shown in Fig. 1, is the muon neutrino survival probability $P_{\mu\mu}$. As was discussed earlier, at high neutrino energies, the muon neutrino will oscillate in a pure two-flavor vacuum scenario with the effective parameters given by Eqs. (25) and (26), since we have used $\theta_{13} = 0$ in the construction of Fig. 1. Furthermore, the choice of $\theta_{13} = 0$ and the approximation that Δm_{21}^2 is small imply that the low-energy neutrinos also oscillate in a two-flavor vacuum scenario, but with the parameters $\Delta m^2 = \Delta m_{31}^2$ and $\theta = \theta_{23}$. In the case of $\beta = 0$, these two cases are obviously equivalent and the matter interaction effects do not

change the situation at any energy (since the $\nu_e\text{-}\nu_e$ element is the only nonzero element of the interaction contribution to the Hamiltonian). However, for $\beta \neq 0$, there will be resonance effects in the region where $\Delta \sim Vv$. As can be seen from Fig. 1, these resonance effects are present mainly around $E \simeq 10^{3.7}$ MeV for $v = 1$ and at energies appropriately displaced from this for $v = 0.5$ and $v = 2$ (*i.e.*, $E \simeq 10^4$ MeV and $E \simeq 10^{3.4}$ MeV, respectively). Note that the colored regions in Figs. 1–5 represent the “exact” (or numerical) three-flavor results, whereas the black solid curves are the approximate two-flavor results given by Eqs. (17)–(20). In general, these two-flavor results are in excellent agreement with the exact three-flavor results, and therefore, they can be used as good approximations in analyses of neutrino data.

B. The electron neutrino survival probability P_{ee}

As discussed in Ref. [19], the electron neutrino survival probability P_{ee} can be a very useful tool when considering ways of determining the small leptonic mixing matrix element U_{e3} . However, as has been discussed earlier in this paper (and also in previous papers [6, 7, 8, 20, 21]), the presence of NSIs can significantly alter the interpretation of a positive oscillation signal in this channel. In particular, the effective two-flavor mixing angle θ' is given by Eq. (10) and the effective matrix element \tilde{U}_{e3} by [6]

$$\tilde{U}_{e3} \simeq U_{e3} + \varepsilon_{e\tau} \frac{2EV}{\Delta m_{31}^2} c_{23}. \quad (27)$$

In Figs. 2 and 3, we present the oscillograms for P_{ee} using different values of β and with $\theta_{13} = 0$ and 8° , respectively. It should be noted that $s' \simeq 0$ in the case when $\theta_{13} = 8^\circ$ and $\beta = \pi/16$ (this is of course the reason for choosing $\theta_{13} = 8^\circ$). As can be observed in these two figures, the high-energy ($E \gtrsim 10^{4.5}$ MeV) behavior of the survival probability P_{ee} is practically unaffected by the change in θ_{13} . This is clearly to be expected, since the vacuum neutrino oscillation terms are suppressed by the neutrino energy E , while the matter interaction terms remain constant. Simply neglecting the vacuum oscillation terms, the expectation at high energy is

$$1 - P_{ee} = \sin^2(2\beta) \sin^2(VvL), \quad (28)$$

which can also be obtained as a limiting case of Eq. (17).

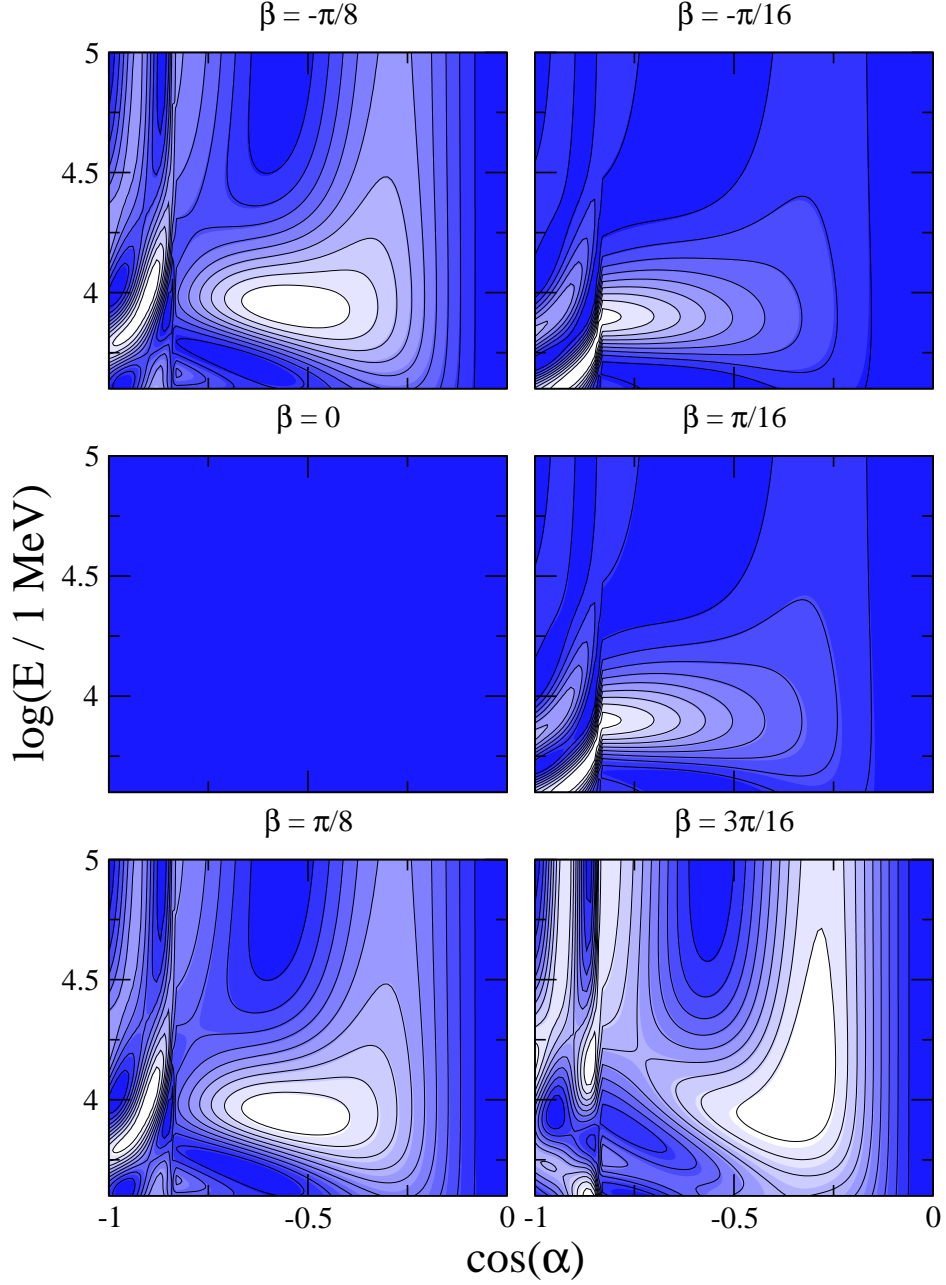


FIG. 2: The electron neutrino survival probability P_{ee} as a function of zenith angle and energy for $\theta_{13} = 0$, $v = 1$, and different values of β . The colored regions and solid black curves are constructed as in Fig. 1.

However, for energies in the resonance regime, the qualitative behavior of P_{ee} is clearly dominated by the value of the effective two-flavor mixing angle θ' . This is particularly apparent in the mid-row panels of Figs. 2 and 3. While the oscillation probability in the

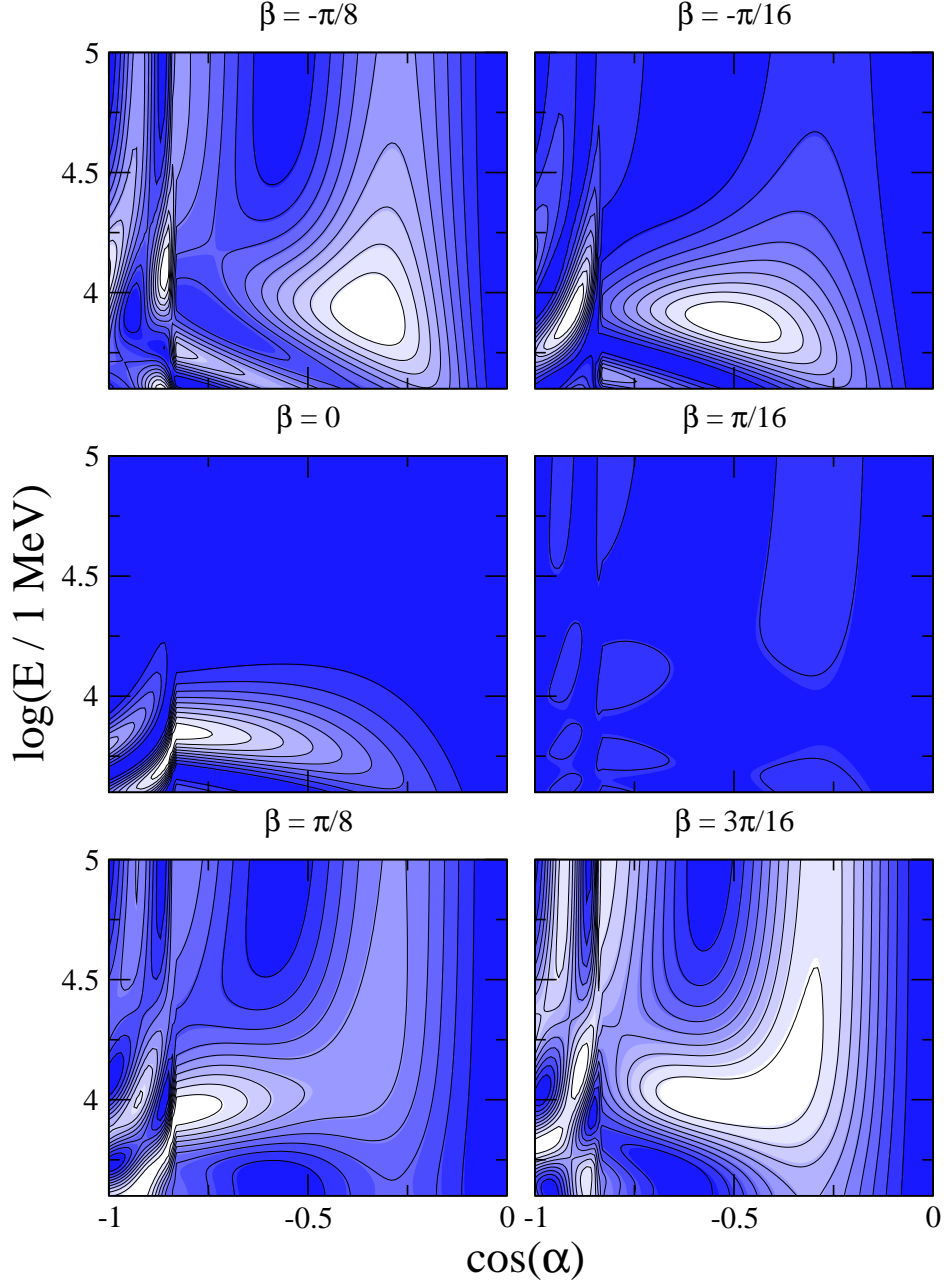


FIG. 3: The same as Fig. 2, but for $\theta_{13} = 8^\circ$.

resonance region is kept small in both the mid-left panel of Fig. 2 and the mid-right panel of Fig. 3 (corresponding to $\theta' \simeq 0$), the resonant behavior at $E \sim 10^{3.8}$ MeV in the mid-right panel of Fig. 2 and the mid-left panel of Fig. 3 (both corresponding to $\theta' \simeq 8^\circ$) are also very similar.

C. The neutrino oscillation probability $P_{e\mu}$

The oscillation of ν_e into ν_μ at neutrino factories has been thoroughly discussed in several papers (see Ref. [22] and references therein) and is commonly known as the “golden” channel. Thus, in Fig. 4, we present oscillograms for the neutrino oscillation probability $P_{e\mu}$ for different values of θ_{13} and β . Comparing this figure with Fig. 3, we can observe that, for $\theta_{13} = 8^\circ$ and $\beta = 0$, half of the oscillating ν_e oscillates into ν_μ . This is a direct result of the leptonic mixing angle θ_{23} being maximal and has been known for a long time (see, *e.g.*, Ref. [23]). However, this is no longer true when $\beta \neq 0$. For the two top panels and the lower-left panel, there are regions where $P_{e\mu} > 0.5$; thus indicating that more than half of the ν_e oscillates into ν_μ in these regions. It should be noted that there is an important caveat, if θ_{23} deviates from maximal mixing, the linear combination of ν_μ and ν_τ , which ν_e oscillates into in the standard framework with nonzero θ_{13} , is not an equal mixture. Therefore, even the standard neutrino oscillation framework can allow for $P_{e\mu} > 0.5$. However, what is important to note is that the ratio $r = P_{e\mu}/P_{e\tau}$ is constant in the standard framework, but depends on both baseline and energy when $\beta \neq 0$. For example, if we consider neutrino oscillations with $\theta_{13} = 8^\circ$ and $\beta = -\pi/16$ at $\cos(\alpha) \simeq 0.3$, then $r = 0$ at high energies due to the decoupling of the ν_μ when the matter interaction terms dominate, while $r > 1$ in the relatively low-energy region around the resonance. Hence, measuring the energy and baseline dependence of r could be a way of determining whether NSIs are present as long as the small mass-squared difference Δm_{21}^2 is negligible. As in the case of the neutrino survival probability P_{ee} , we can observe that there are practically no oscillations in the resonance region for the cases where $\theta' \simeq 0$.

D. The neutrino oscillation probability $P_{\mu\tau}$

In order to accommodate all of Eqs. (17)–(20) in our numerical study, we also show the results for the neutrino oscillation probability $P_{\mu\tau}$ in Fig. 5. Again, we can observe the fact that the oscillations for given values of θ' turn out to be very similar. Especially, the panels where $\theta' \simeq 0$ are almost identical and very similar to pure vacuum neutrino oscillations. In particular, the effects of going from mantle-only trajectories to core-crossing trajectories at about $\cos(\alpha) \simeq 0.84$ is not apparent in these figures, the reason being the fact that the

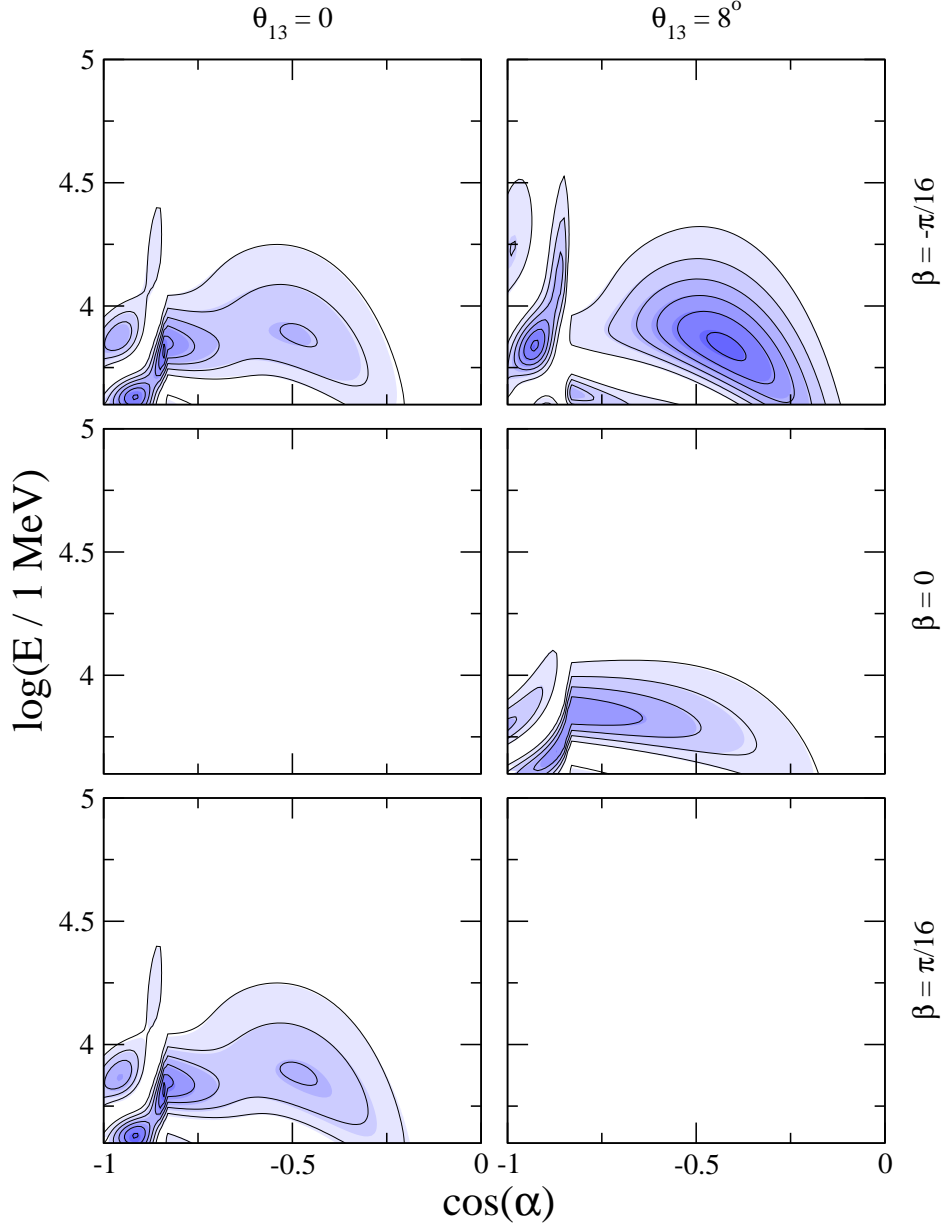


FIG. 4: The neutrino oscillation probability $P_{e\mu}$ as a function of zenith angle and energy for different values of θ_{13} and β . For this figure, we have used $v = 1$ and the colored regions and solid black curves are constructed as in Fig. 1.

Hamiltonian is diagonalized by the matrix $(V_{\alpha i})$ given in Eq. (14) for all values of VE .

It should also be noted that $P_{\mu e} = P_{e\mu}$, since we use a symmetric matter density profile and no CP -violating phases in this section. Thus, the differences between the figures for the $P_{\mu\mu}$ probabilities and those for the $P_{\mu\tau}$ probabilities (except for the interchange of dark and

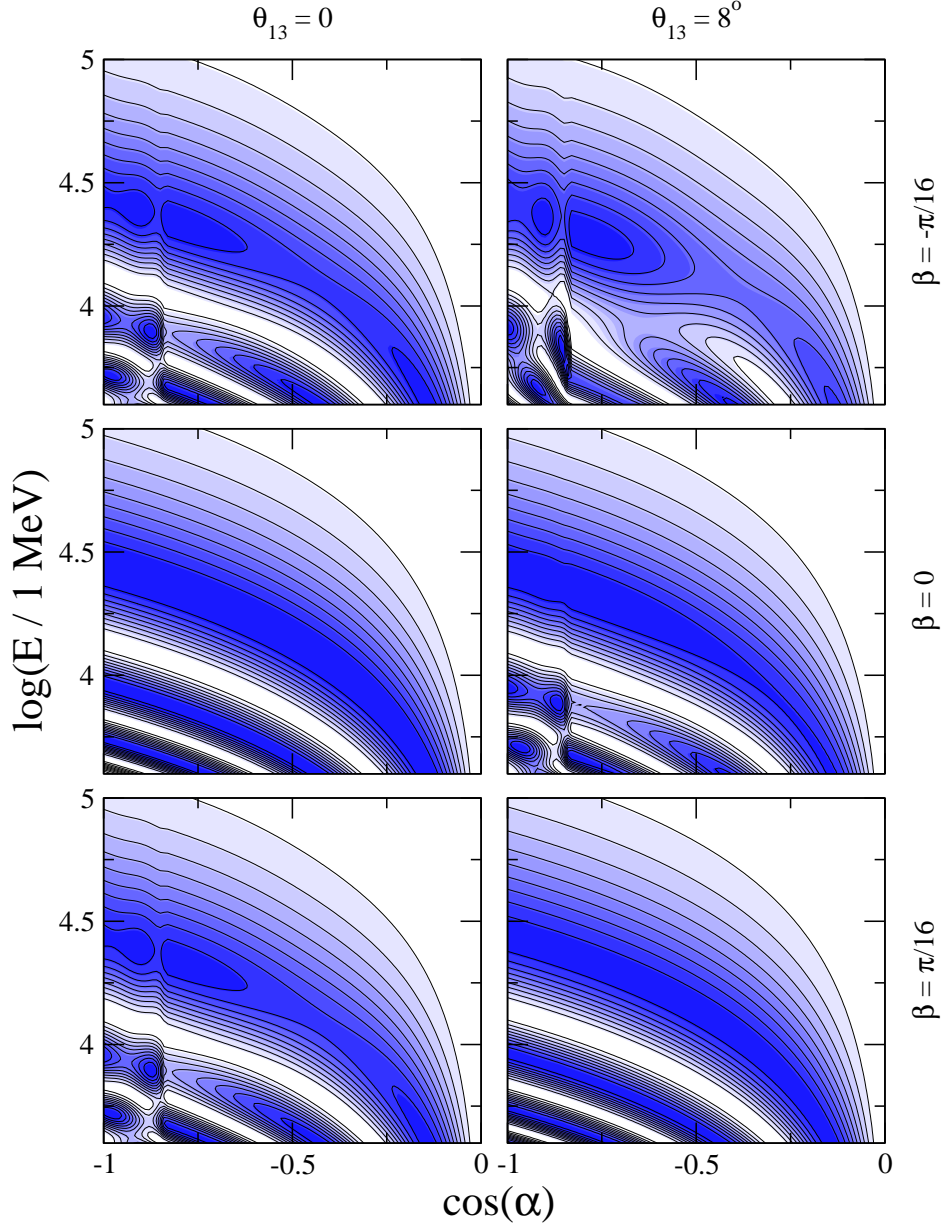


FIG. 5: The neutrino oscillation probability $P_{\mu\tau}$ as a function of zenith angle and energy for different values of θ_{13} and β . For this figure, we have used $v = 1$ and the colored regions and solid black curves are constructed as in Fig. 1.

light areas) are summarized in the figures for the $P_{e\mu}$ probabilities as $P_{\mu e} + P_{\mu\mu} + P_{\mu\tau} = 1$.

V. APPLICATION TO A FICTIVE NEUTRINO FACTORY

In this section, we study the impact of NSIs on the sensitivity contours of a fictive neutrino factory experiment. In order to achieve this, we have used the General Long-Baseline Experiment Simulator (GLOBES) [24, 25] and a modified version of the standard neutrino factory experimental setup included in the GLOBES distribution (essentially “NuFact-II” from Ref. [26]), modified to only take the ν_μ disappearance channel into account and to have a baseline of $L = 7000$ km (from Fig. 1, we note that the NSI effects should be relatively strong at this baseline, it is also very close to the “magic” baseline [27], which means that the impact of the solar parameters is expected to be small). This neutrino factory setup corresponds to a parent muon energy of 50 GeV and an assumed target power of 4 MW. The running time is set to four years in each polarity and the detector is assumed to be a magnetized iron calorimeter with a fiducial mass of 50 kton. For the neutrino cross-sections, we have also used the files included in the GLOBES distribution, which are based on Refs. [28, 29]. We consider neutrino energies in the range 4–50 GeV, divided into 20 equally spaced energy bins. The simulated neutrino oscillation parameters are the same as in the previous section, *i.e.*, they are given in Table I. The simulated θ_{13} has been put to zero for simplicity.

A. Determination of standard parameters

One important question when considering NSIs is how the inclusion of NSIs can alter the sensitivity of an experiment. This subject has been studied for a number of different neutrino oscillation experiments [4, 5, 6, 7, 9, 20, 21, 30, 31]. At the neutrino factory in question, the ν_μ disappearance channel will normally be a very sensitive probe to the neutrino oscillation parameters Δm_{31}^2 and θ_{23} . However, with the inclusion of NSIs, there is an additional degeneracy, leading to experiments becoming less sensitive to the standard neutrino oscillation parameters. Note that this degeneracy has been investigated before in the case of atmospheric neutrinos in Refs. [4, 5]. In particular, the major part of the neutrino energies at the neutrino factory described before are well above the resonance energy. Thus, the induced degeneracy in the $\sin^2(\theta_{23})-\Delta m_{31}^2$ plane should be well described by Eqs. (23) and (24).

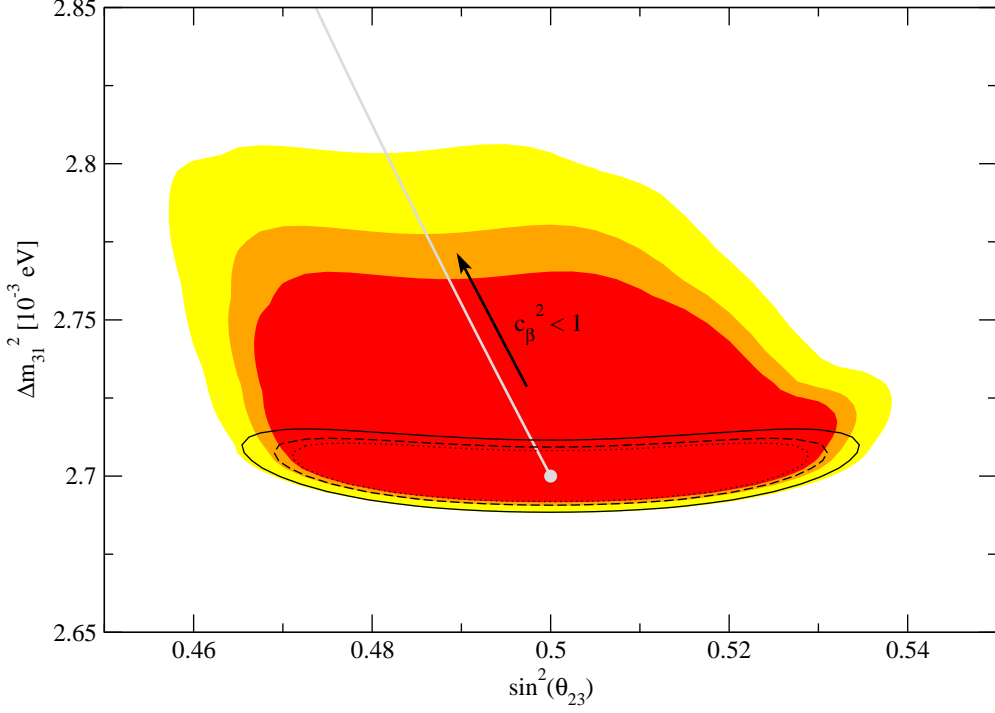


FIG. 6: The sensitivity contours (2 d.o.f.) in the $\sin^2(2\theta_{23})-\Delta m_{31}^2$ plane for the ν_μ disappearance channel at the fictive neutrino factory experiment described in the text. The black curves correspond to the sensitivity if it is assumed that there are no NSIs present, while the colored regions correspond to the sensitivity if NSIs within current bounds are taken into account. The gray circle corresponds to the simulated parameters and the gray curve to the expected direction of the NSI degeneracy. The confidence levels are 90 %, 95 %, and 99 %, respectively. We have assumed Gaussian priors of $\varepsilon_{ee} < 2.6$, $\varepsilon_{e\tau} < 1.9$, and $\varepsilon_{\tau\tau} < 1.9$ at a 90 % confidence level.

In Fig. 6, we can observe how this degeneracy manifests itself in the sensitivity of the ν_μ disappearance channel. While the sensitivity contours are symmetric around $\sin^2(\theta_{23}) = 0.5$ when not including NSIs (*i.e.*, $\beta = 0$), they extend to smaller values of θ_{23} and larger values of Δm_{31}^2 when NSIs are included (*i.e.*, $\beta \neq 0$). The conclusion that the sensitivity contours will extend to smaller θ_{23} and larger Δm_m^2 is general and apparent from the form of Eqs. (23) and (24), where the same θ_m and Δm_m^2 can be achieved for a class of different θ_{23} and Δm_{31}^2 given by

$$\tan(\theta_{23}) = c_\beta \tan(\theta_m), \quad (29)$$

$$\Delta m_{31}^2 = \frac{\Delta m_m^2}{1 - s_\beta^2 c_{23}^2}, \quad (30)$$

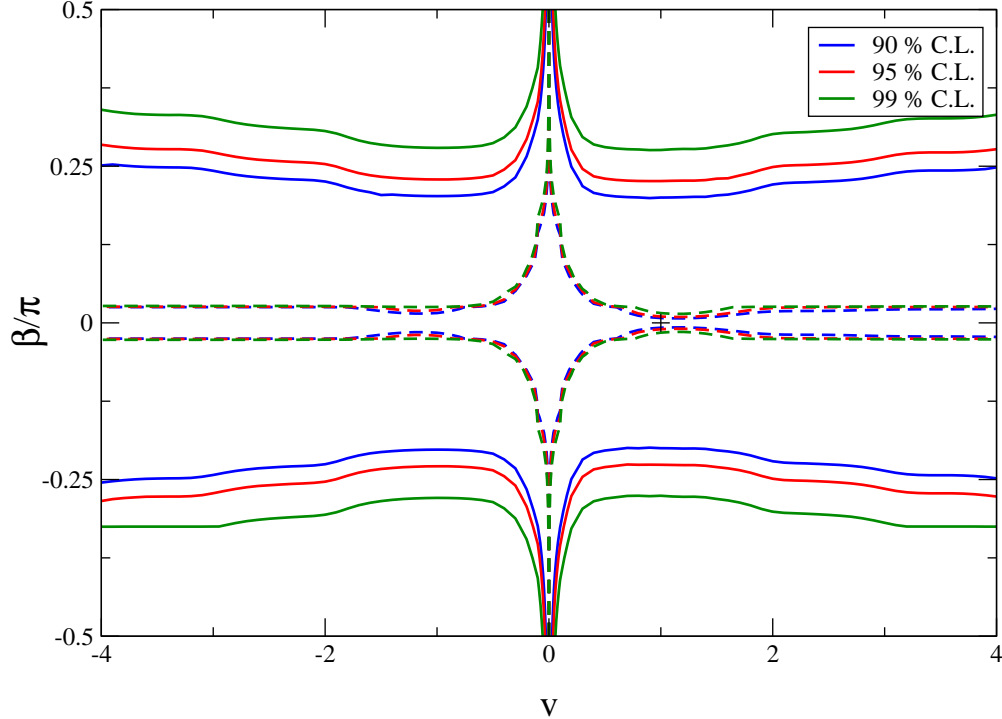


FIG. 7: The sensitivity (2 d.o.f.) to the NSI parameters v and β for the ν_μ disappearance channel at the fictive neutrino factory experiment described in the text. The dashed curves are the systematics-only sensitivities and the solid curves include parameter correlations with the standard neutrino oscillation parameters (with errors comparable to the current errors). The contours were constructed assuming no NSIs and the $+$ corresponds to this situation.

in the case when $\theta_{13} = 0$. This degeneracy has also been marked in Fig. 6 for θ_{23} and Δm_{31}^2 equal to the simulated values when $\beta = 0$.

B. Determination of NSI parameters

Another interesting question in relation to NSIs and future experiments is what the experimental sensitivity to NSIs is, *e.g.*, what bounds the experiments could put on the NSI parameters. Thus, in Fig. 7, we show the sensitivity contours in the v - β plane (the other NSI parameters have been marginalized) corresponding to the ν_μ disappearance channel at a neutrino factory described above. From this figure, we notice that the given experiment is not very sensitive to the NSI parameters as long as the knowledge on the standard neutrino oscillation parameters has errors which are comparable to those of the current experimen-

tal bounds. Essentially, for large v (such that the entire energy spectrum is well above resonance), the bound on β comes from the mismatch between the effective θ_m and Δm_m^2 measured by the neutrino factory and the external measurements on θ_{23} and Δm_{31}^2 and the errors of both are propagated to the error in the determination of β . However, if the external errors on the standard neutrino oscillation probabilities are very small (*i.e.*, such that we do not need to consider correlations with the standard parameters), then the bounds on the NSI parameters are significantly improved. It should be noted that the insensitivity to β for small $|v|$ is clearly due to the fact that it is not possible to determine β when the interaction effects are suppressed. We should also note that the given experiment is clearly not the best to use in order to distinguish NSIs from standard neutrino oscillations. For example, it should be more viable to detect NSIs through other oscillation channels or through the combination of the ν_μ disappearance channel with one of the appearance channels.

VI. SUMMARY AND CONCLUSIONS

We have considered the effects of NSIs on the propagation of \geq GeV neutrinos in the Earth with the assumption that Δm_{21}^2 is small and that ε_{ee} , $\varepsilon_{e\tau}$, and $\varepsilon_{\tau\tau}$ are the only important NSI parameters. We have shown that, if the NSI parameters are constrained to be on the “atmospheric parabola,” then the neutrino flavor evolution matrix can be straightforwardly computed using a simple two-flavor scenario in matter with a mixing angle given by Eq. (10). This two-flavor scenario is the natural NSI extension of the usual two-flavor approximation used in standard neutrino oscillations when Δm_{21}^2 is small. While this two-flavor scenario, unlike the standard two-flavor scenario, is not diagonal in flavor space, it should be noted that if NSI effects are present in the propagation, then they should also be present in the creation and detection processes, meaning that the actual flavor space is no longer equivalent to the weak interaction flavor space. Deviations from the atmospheric parabola or other NSI parameters can be easily treated as a perturbation to the two-flavor scenario.

The impact of NSIs on neutrino oscillations in the Earth as well as the accuracy of our two-flavor approximation have been studied using neutrino oscillograms of the Earth. It was noted that the resonance regions in the neutrino survival channels are mainly dependent on the mixing angle of the effective two-flavor scenario, implying a degeneracy between θ_{13} and the NSI angle β . This degeneracy is preferentially broken by using data from above or below

the resonance, or by studying the flavor combination into which neutrinos actually oscillate.

Finally, we have given an example of the impact of the NSIs in a fictive neutrino factory with a baseline of $L = 7000$ km studying the muon neutrino disappearance channel. We have shown that the degeneracy between the standard and NSI parameters extends in the expected direction and computed the actual sensitivity to the NSI parameters, both by assuming no degeneracy with the standard parameters (*i.e.*, the standard parameters assumed to be exactly known) and by assuming correlations with the standard parameters (in this case, Gaussian priors with a size corresponding to the current experimental errors were used). Again, it should be stressed that this part is only intended to show the impact of the NSI parameters in a fictive experiment and does not offer a realistic approach for searching for NSIs. Such considerations can be found in Ref. [30].

Acknowledgments

We would like to thank Evgeny Akhmedov for useful discussions. This work was supported by the Swedish Research Council (Vetenskapsrådet), Contract Nos. 623-2007-8066 (M.B.) and 621-2005-3588 (T.O.) and the Royal Swedish Academy of Sciences (KVA) (T.O.).

-
- [1] L. Wolfenstein, Phys. Rev. **D17**, 2369 (1978).
 - [2] S. P. Mikheyev and A. Y. Smirnov, Sov. J. Nucl. Phys. **42**, 913 (1985).
 - [3] S. P. Mikheyev and A. Y. Smirnov, Nuovo Cim. **C9**, 17 (1986).
 - [4] A. Friedland, C. Lunardini, and M. Maltoni, Phys. Rev. **D70**, 111301 (2004), hep-ph/0408264.
 - [5] A. Friedland and C. Lunardini, Phys. Rev. **D72**, 053009 (2005), hep-ph/0506143.
 - [6] M. Blennow, T. Ohlsson, and J. Skrotzki, Phys. Lett. **B660**, 522 (2008), hep-ph/0702059.
 - [7] A. Friedland and C. Lunardini, Phys. Rev. **D74**, 033012 (2006), hep-ph/0606101.
 - [8] N. Kitazawa, H. Sugiyama, and O. Yasuda (2006), hep-ph/0606013.
 - [9] A. Esteban-Pretel, P. Huber, and J. W. F. Valle, Phys. Lett. **B668**, 197 (2008), 0803.1790.
 - [10] S. Davidson, C. Peña-Garay, N. Rius, and A. Santamaria, JHEP **03**, 011 (2003), hep-ph/0302093.
 - [11] J. Abdallah et al. (DELPHI), Eur. Phys. J. **C38**, 395 (2005), hep-ex/0406019.

- [12] M. Blennow and T. Ohlsson, Phys. Lett. **B609**, 330 (2005), hep-ph/0409061.
- [13] P. I. Krastev and A. Y. Smirnov, Phys. Lett. **B226**, 341 (1989).
- [14] Q. Y. Liu, S. P. Mikheyev, and, A. Y. Smirnov, Phys. Lett. **B440**, 319 (1998), hep-ph/9803415.
- [15] S. T. Petcov, Phys. Lett. **B434**, 321 (1998), hep-ph/9805262.
- [16] E. K. Akhmedov, Nucl. Phys. **B538**, 25 (1999), hep-ph/9805272.
- [17] E. K. Akhmedov, A. Dighe, P. Lipari, and, A. Y. Smirnov, Nucl. Phys. **B542**, 3 (1999), hep-ph/9808270.
- [18] E. K. Akhmedov, M. Maltoni, and, A. Y. Smirnov, Phys. Rev. Lett. **95**, 211801 (2005), hep-ph/0506064.
- [19] E. K. Akhmedov, M. Maltoni, and A. Y. Smirnov, JHEP **05**, 077 (2007), hep-ph/0612285.
- [20] P. Huber, T. Schwetz, and J. W. F. Valle, Phys. Rev. Lett. **88**, 101804 (2002), hep-ph/0111224.
- [21] M. Blennow, T. Ohlsson, and W. Winter, Eur. Phys. J. **C49**, 1023 (2007), hep-ph/0508175.
- [22] A. Bandyopadhyay et al. (ISS Physics Working Group) (2007), 0710.4947.
- [23] E. K. Akhmedov (1999), hep-ph/0001264.
- [24] P. Huber, M. Lindner, and W. Winter, Comput. Phys. Commun. **167**, 195 (2005), hep-ph/0407333.
- [25] P. Huber, J. Kopp, M. Lindner, M. Rolinec, and W. Winter, Comput. Phys. Commun. **177**, 432 (2007), hep-ph/0701187.
- [26] P. Huber, M. Lindner, and W. Winter, Nucl. Phys. **B645**, 3 (2002), hep-ph/0204352.
- [27] P. Huber and W. Winter, Phys. Rev. **D68**, 037301 (2003), hep-ph/0301257.
- [28] M. D. Messier (1999), UMI-99-23965.
- [29] E. A. Paschos and J. Y. Yu, Phys. Rev. **D65**, 033002 (2002), hep-ph/0107261.
- [30] J. Kopp, T. Ota, and W. Winter, Phys. Rev. **D78**, 053007 (2008), 0804.2261.
- [31] M. Blennow, D. Meloni, T. Ohlsson, F. Terranova, and M. Westerberg, Eur. Phys. J. **C56**, 529 (2008), 0804.2744.